IN-SILICO STUDIES OF MTNB, TM14A, LEG2, S10A3 AND LTC4S PROTEINS INVOLVED IN LUNG CANCER

Ms. Mini Fernandez
Assistant Professor
Department of Biotechnology,
St. Francis College for Women, Hyderabad

Ms. ANVSL Sarayu
Department of Biotechnology,
St. Francis College for Women, Hyderabad

https://doi.org/10.34293/ctbtls.2025.ch008

Abstract

Lung cancer has the highest mortality rates among both men and women and is the leading cause of cancer-related deaths worldwide. Research has shown that five proteins – MTNB, TM14A, LEG2, S10A3, and LTC4S – can accelerate the development of lung cancer. These proteins' target sequences, template sequences, and alignments were obtained from UniProtKB, PDB-RCSB, and ClustalOmega. Protein modeling and validation were performed using SWISS-MODEL and the SAVES v6.0 and ProSA tools. Surface pockets were identified using CASTpFold. Each protein was then docked with three selected ligands – sorafenib, distamycin, and sunitinib – using Vina in "PyRx." AutoDock Vina facilitated the separation of ligand conformations. Finally, BIOVIA Discovery Studio was used to visualize the interactions between the proteins and the drugs. Understanding these interactions highlights the potential of these medications as targeted therapies that could reduce tumor growth and improve patient outcomes.

Keywords: *Lung cancer, UniProtKB, PDB-RCSB, Vina, interactions.*

Introduction

One kind of cancer that begins when aberrant cells proliferate in the lungs out of control is lung cancer. With the greatest death rates among both men and women, lung cancer is the primary cause of cancer-related fatalities globally. Squamous cell carcinoma, carcinoid, nonsquamous non-small cell lung cancer, and small cell carcinoma are the four primary forms of lung cancer. NSCLCs account for 85–90% of these lung malignancies. Squamous cell carcinoma, which accounts for 25% to 30% of lung cancers, adenocarcinoma, which accounts for roughly 40% of lung cancers, and big cell carcinoma, which accounts for 10% to 15% of lung cancers, are the subtypes of this diverse group. SCLC, which makes up 10% to 15% of all lung cancers, is the second most common kind. Carcinoid tumors, which make up 1% to 2% of lung tumors, are among the additional tumors that can develop in the lungs in addition to the two primary forms of lung cancer (Gilad, 2012). The symptoms can include cough, dyspnea, hoarseness, chest pain, wheezing, hemoptysis, nausea or vomiting, swelling of the face and arms, anorexia, weight loss, fatigue, bone pain, clubbing, headache, and seizures (Yoder, 2006).

Spiral CT scans have the advantage of continuously collecting data, which reduces radiation exposure, accelerates the scanning process, and enhances diagnostic accuracy

compared to plain radiography. LDCT can also detect false positives, meaning abnormalities that are not related to cancer. Another method for diagnosing lung cancer is through the cytological analysis of sputum, particularly with multiple samples. This approach helps in identifying core tumors located in the larger bronchi.

The most widely used diagnostic procedure for obtaining a definitive histological diagnosis of lung cancer is white light bronchoscopy (WLB). Ultimately, a tissue biopsy remains the gold standard for confirming the presence of cancer (Nooreldeen, 2021). Adjuvant therapy, paired with surgical tumor excision, is the recommended treatment for stage I or II NSCLC. In contrast, chemotherapy and radiation therapy are used to treat the disease at stages III and IV. Nanocarrier-based drug delivery has emerged as a cutting-edge approach for treating lung cancer, offering significant advantages such as enhanced safety through targeted administration of anticancer medications and improved drug absorption in the body. Numerous receptor tyrosine kinases, including EGFR, c-Met, and ALK, are vital targets for molecular targeted therapy, as they play a key role in cell growth and survival. Immunotherapy techniques, such as checkpoint inhibitors, are safe, and effective, and may offer additional treatment options for NSCLC patients (Li, 2023).

It was discovered that non-small cell lung carcinoma cells and tumors have down-regulated APIP (human mtnb) at the mRNA and protein levels (Mary, 2012). Lung adenocarcinoma (LUAD) tumor tissues showed significantly higher levels of TMEM14A mRNA expression compared to normal tissues. TMEM14A plays a crucial role in promoting the growth of non-small cell lung cancer (NSCLC) cells. Additionally, the involvement of TMEM14A in mitochondrial ATP synthesis may be associated with the development of NSCLC (Jang, 2023). Galectins play a significant role in cancer development by influencing apoptosis, tumor invasion, angiogenesis, cell adhesion during metastasis, and the immune response to tumors (Chang, 2017). Hoskin et al. have found that the lungs of individuals with respiratory disorders and the saliva of healthy persons exhibit oxidative cross-linking through the disulfide bonds of S100 proteins (Messana, 2023). Leukotrienes are found in higher quantities in the pulmonary arterioles of patients with PAH and the airways of patients with asthma and COPD. The severity of the condition is correlated with these leukotriene levels. Immune cell migration into the lungs is stimulated by leukotriene overexpression and subsequent contact with its receptors (Tian, 2020).

Materials and Methods

Homology modeling: The biological databases NCBI, BLAST, PDB-RCSB, UniProtKB, and Clustal Omega were used to select the target and template proteins and to assess the conserved domains. The selection criteria for target sequences included proteins with fewer than 250 amino acids, those that had been reviewed, and those associated with relevant publications. Proteins were selected based on a percentage identity greater than 27% and a query coverage exceeding 70%. If the requirements were met, the 4-letter PDB accession codes were noted to access in PDB-RCSB. The unmodeled regions were assessed in PDB and those with minimal or no unmodeled regions were selected as template proteins.

Model generation and validation: A variety of tools were utilized to generate and validate the model. SWISS-MODEL is a free online program that predicts a protein's three-dimensional structure based on its amino acid sequence through homology modeling. PROSA is an interactive tool designed to detect defects in 3D protein structures.

Additionally, SAVES v6.1 is a comprehensive toolkit that includes several tools—ERRAT, VERIFY3D, PROVE, PROCHECK, and WHATCHECK—for assessing various stereochemical characteristics of protein structures.

Active Site Prediction: The active sites of the generated models were predicted using the Computed Atlas of Surface Topography of the Universe of Protein Folds (CASTpFold). This online tool utilizes theoretical and algorithmic results from computational geometry to analytically identify protein pockets and cavities.

Selection of Ligands: Ligands for molecular docking were chosen from PubChem, an open chemistry database maintained by the National Institutes of Health (NIH). This database contains a wealth of information, including chemical structures, identifiers, chemical and physical properties, biological activities, patents, as well as health, safety, and toxicity data. The selected ligands include Distamycin, Sunitinib, and Sorafenib.

Docking of Ligand and Macromolecule: Docking was performed using PyRx, a virtual screening software designed for Computational Drug Discovery. This tool can screen libraries of compounds against potential drug targets. To split the ligand conformations, Autodock Vina was utilized via the command prompt.

Visualization of Interactions between Ligands and Proteins: The BIOVIA Discovery Studio Visualizer was employed to analyze the interactions between the ligands and the proteins.

Results and Discussion

Homology Modeling: Selection of target proteins: The accession codes NP_057041.2, NP_054770.1, NP_006489.1, NP_002951.1, and NP_665874.1 were obtained from NCBI to retrieve the FASTA sequences for five proteins: Methylthioribulose-1-phosphate dehydratase, Transmembrane Protein 14A, Galectin-2, Protein S100-A3, and Leukotriene C4 Synthase from UniProtKB. NCBI provides genomic data in the format of FASTA (Kitts, 2016). To provide protein sequences and functional data, the SIB, EBI, and PIR established the Universal Protein Resource Consortium (UniProt) (Boutet, 2016). The resulting FASTA sequences were then utilized for homology modeling.

Selection of template proteins: The protein accession codes 4M6R, 2LOO, 5DG1, 1KSO, and 2PNO were searched in PDB-RCSB to retrieve the sequences. The Protein Data Bank is the sole global repository for structural data of biological macromolecules (Berman, 2000).

Multiple sequence alignment: Multiple sequence alignment was performed using Clustal Omega with the output format set to 'ClustalW with character counts' was done. Protein alignments are highly accurate and can be completed quickly enough to create very large alignments (Sievers, 2018).

Model Generation: The FASTA sequences of the target proteins were pasted in SWISS-MODEL to generate the models in PDB format. The models with high GMQE numbers were

downloaded in PDB format. Its modeling capabilities include modeling homo and heteromeric complexes using the interacting partners' amino acid sequences as a starting point (Waterhouse, 2018).

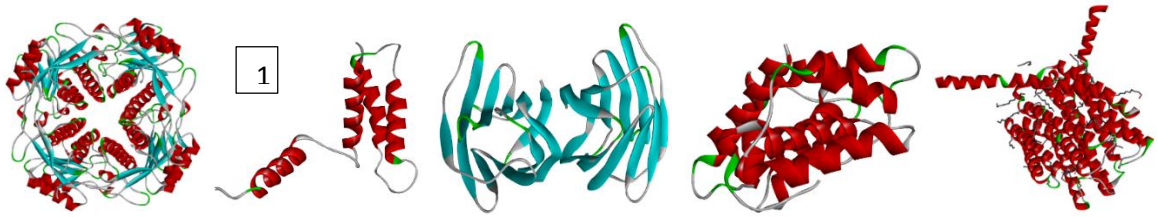

Figure1: Structures of MTNB, TM14A, LEG2, S10A3, and LTC4S Generated using SWISS-MODEL

Model Validation: The modeled proteins were uploaded in SAVES v6.1 and ProSa and the scoring results from VERIFY 3D, PROCHECK summary, Ramachandran plots, Local model quality, and Overall model quality for the generated models are as follows:

VERIFY 3D establishes if an atomic 3D model is compatible with its amino acid sequence. PROCHECK uses both the overall structural geometry and residue-by-residue geometry to assess the stereochemical quality of a protein structure. A Ramachandran plot can provide a basic initial check (Pradeepkiran, 2021). The Z-score, which measures how well a protein structure model matches the expected energy distribution of native proteins of comparable size, is the main metric used to evaluate the overall quality of the model. A plot of local quality scores is used to identify problematic areas of a model (Wiederstein, 2007).

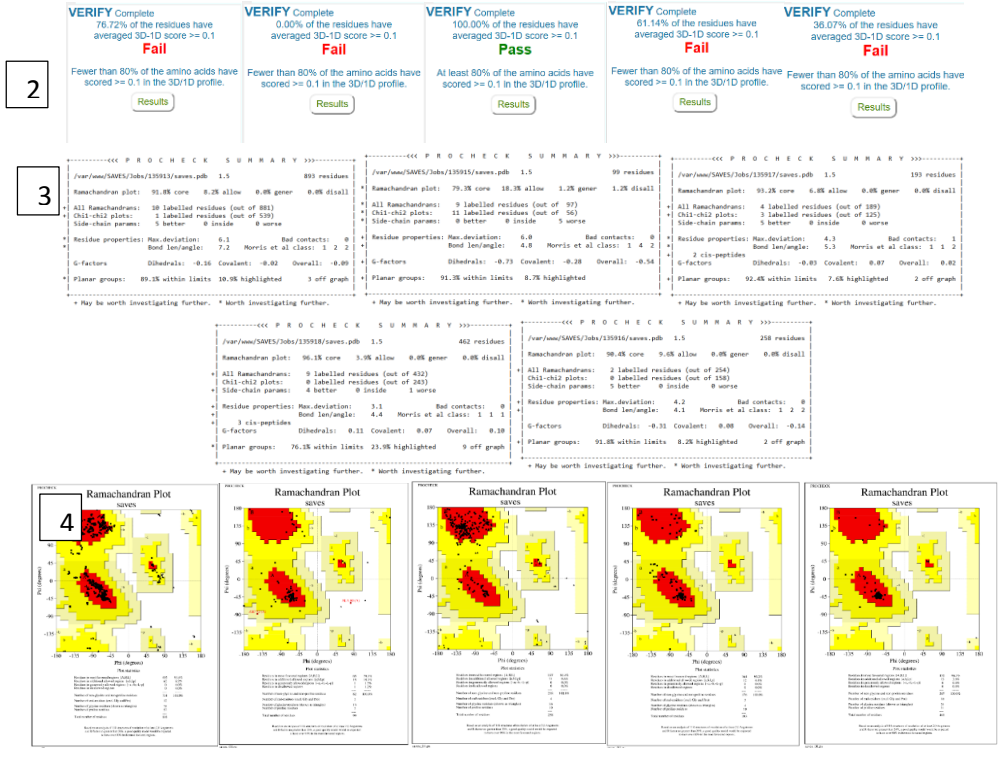

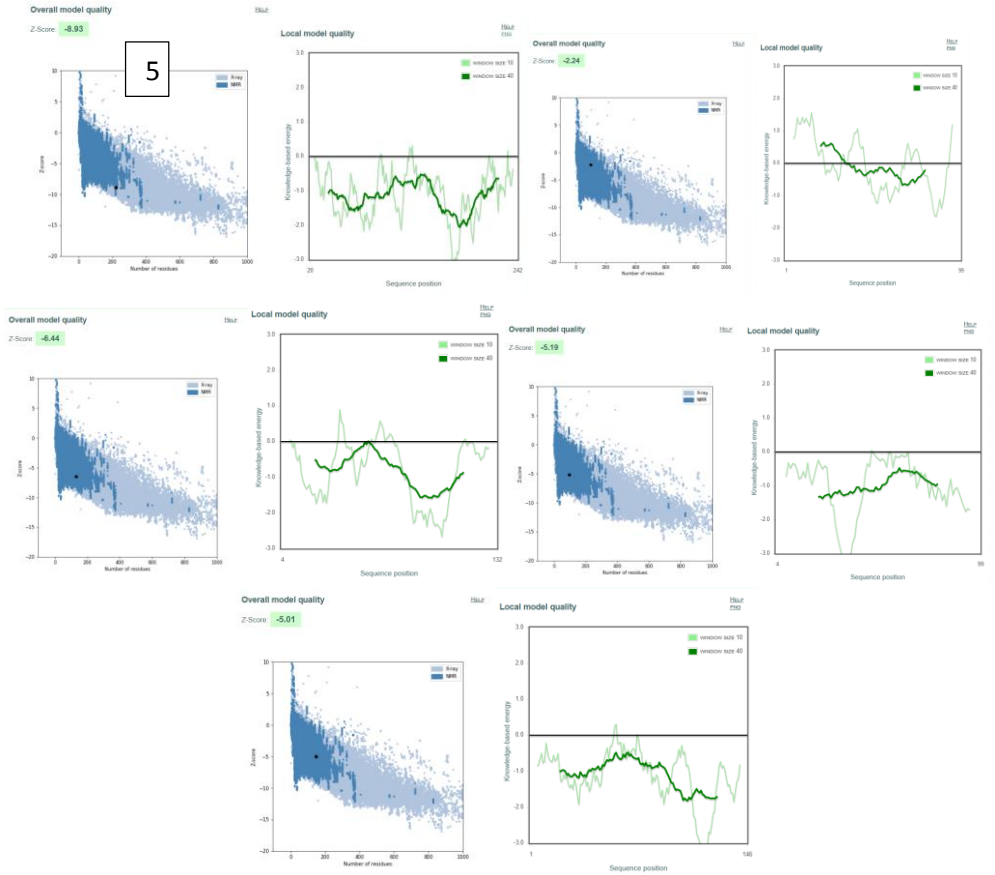

Figures 2, 3, 4, and 5: Model validation results of MTNB, TM14A, LEG2, S10A3, and LTC4S generated using SAVESv6.1 and ProSa

Active site prediction: The active sites in the generated models were predicted using CASTpFold this platform provides information on non-singleton representative structures derived from AlphaFold2, including details about interior cavities, surface pockets, and interconnecting channels, among other features (Ye, 2024).

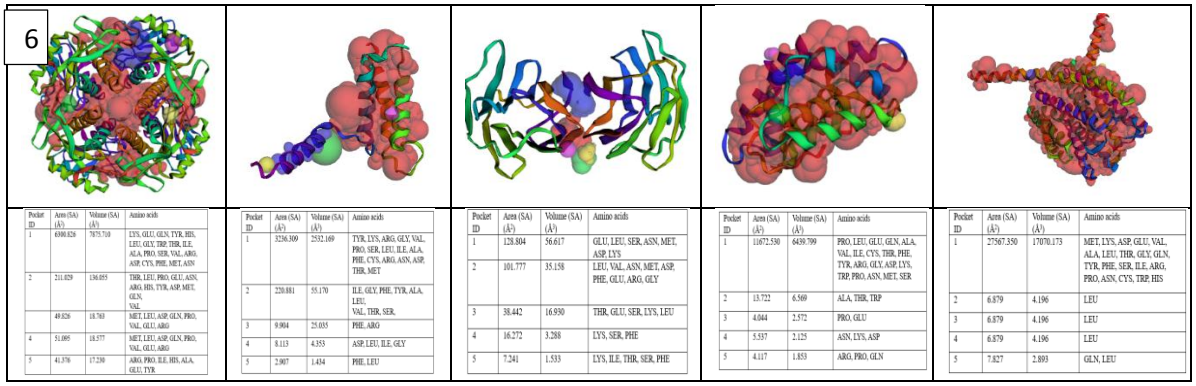

Pocket ID	Area (SA) (Å²)	Volume (SA) (Å³)	Amino acids
1	6300.828	7875.710	LYS, GLU, GLN, TYR, HIS, LEU, GLY, TRP, THR, ILE, ALA, PRO, SER, VAL, ARG, ASP, CYS, PHE, MET, ASN
2	211.029	136.055	THR, LEU, PRO, GLU, ASN, ARG, HIS, TYR, ASP, MET, GLN, VAL
	49.028	18.763	MET, LEU, ASP, GLN, PRO, VAL, GLU, ARG
4	51.095	18.577	MET, LEU, ASP, GLN, PRO, VAL, GLU, ARG
5	41.376	17.230	ARG, PRO, ILE, HIS, ALA, GLU, TYR

Pocket ID	Area (SA) (Å²)	Volume (SA) (Å³)	Amino acids
1	3236.309	2532.169	TYR, LYS, ARG, GLY, VAL, PRO, SER, LEU, ILE, ALA, PHE, CYS, ARG, ASN, ASP, THR, MET
2	220.881	55.170	ILE, GLY, PHE, TYR, ALA, LEU, VAL, THR, SER,
3	9.904	25.035	PHE, ARG
4	8.113	4.353	ASP, LEU, ILE, GLY
5	2.907	1.434	PHE, LEU

Pocket ID	Area (SA) (Å²)	Volume (SA) (Å³)	Amino acids
1	128.804	56.617	GLU, LEU, SER, ASN, MET, ASP, LYS
2	101.777	35.158	LEU, VAL, ASN, MET, ASP, PHE, GLU, ARG, GLY
3	38.442	16.930	THR, GLU, SER, LYS, LEU
4	16.272	3.288	LYS, SER, PHE
5	7.241	1.533	LYS, ILE, THR, SER, PHE

Pocket ID	Area (SA) (Å²)	Volume (SA) (Å³)	Amino acids
1	11672.530	6439.799	PRO, LEU, GLU, GLN, ALA, VAL, ILE, CYS, THR, PHE, TYR, ARG, GLY, ASP, LYS, TRP, PRO, ASN, MET, SER
2	13.722	6.569	ALA, THR, TRP
3	4.044	2.572	PRO, GLU
4	5.537	2.125	ASN, LYS, ASP
5	4.117	1.853	ARG, PRO, GLN

Pocket ID	Area (SA) (Å²)	Volume (SA) (Å³)	Amino acids
1	27567.350	17070.173	MET, LYS, ASP, GLU, VAL, ALA, LEU, THR, GLY, GLN, TYR, PHE, SER, ILE, ARG, PRO, ASN, CYS, TRP, HIS
2	6.879	4.196	LEU
3	6.879	4.196	LEU
4	6.879	4.196	LEU
5	7.827	2.893	GLN, LEU

Figure 6: Results of pockets, area, volume, and amino acid residues of MTNB, TM14A, LEG2, S10A3, and LTC4S generated using CASTpFold

Selection of Ligands: Three drugs Distamycin, Sunitinib, and Sorafenib used to treat lung cancer were selected through a literature review in PubMed and then their 2D & 3D structures were obtained from PubChem.

Docking of Ligand and Macromolecule: The three ligands selected were docked to each protein using Vina in PyRx and after the program was run the results containing the binding affinity and RMSD values were obtained.

Visualization of interactions between ligands and proteins: The interactions between the drugs and each protein were visualized in both two-dimensional and three-dimensional formats using Discovery Studio. In the open conformational environment of protein structures, weak intermolecular interactions like hydrophobic and hydrogen bonding are essential for maintaining energetically favored ligands (Patil, 2010).

MTNB and Distamycin

7

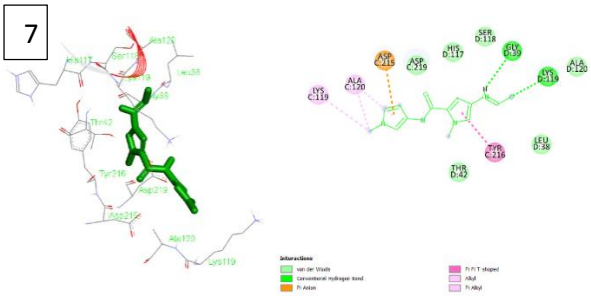

NAME	DISTANCE	CATEGORY	TYPES
:UNK0:H58 - D:GLY39:O	2.76174	Hydrogen Bond	Conventional Hydrogen Bond
D:LYS119:HN - :UNK0:O4	2.30076	Hydrogen Bond	Conventional Hydrogen Bond
C:ASP215:OD2 - :UNK0	4.49967	Electrostatic	Pi-Anion
:UNK0 - C:TYR216	5.12925	Hydrophobic	Pi-Pi T-shaped
:UNK0:C26 - C:LYS119	3.69147	Hydrophobic	Alkyl
:UNK0:C26 - C:ALA120	3.69165	Hydrophobic	Alkyl
:UNK0 - C:ALA120	4.45373	Hydrophobic	Pi-Alkyl

MTNB and Sunitinib

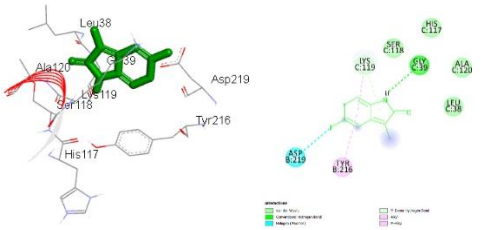

NAME	DISTANCE	CATEGORY	TYPES
:UNK0:H53 - C:GLY39:O	2.34962	Hydrogen Bond	Conventional Hydrogen Bond
B:ASP219:OD2 - :UNK0:F1	3.2855	Halogen	Halogen (Fluorine)
C:LYS119:HN - :UNK0	3.1929	Hydrogen Bond	Pi-Donor Hydrogen Bond
C:LYS119 - :UNK0	4.42781	Hydrophobic	Alkyl
:UNK0 - C:LYS119	4.20531	Hydrophobic	Pi-Alkyl
B:TYR216 - :UNK0	5.47359	Hydrophobic	Pi-Alkyl

MTNB and Sorafenib

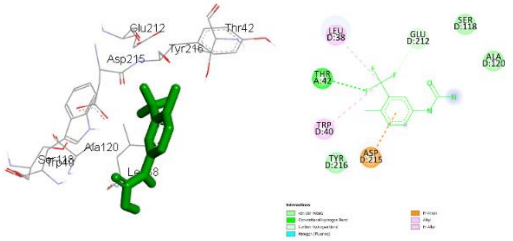

NAME	DISTANCE	CATEGORY	TYPES
A:THR42:HG1 - :UNK0:F2	2.57591	Hydrogen Bond; Halogen	Conventional Hydrogen Bond; Halogen (Fluorine)
D:GLU212:CA - :UNK0:F4	3.54226	Hydrogen Bond; Halogen	Carbon Hydrogen Bond; Halogen (Fluorine)
D:GLU212:O - :UNK0:F4	3.55266	Halogen	Halogen (Fluorine)
D:ASP215:OD2 - :UNK0	3.51567	Electrostatic	Pi-Anion
:UNK0:C25 - D:LEU38	4.48379	Hydrophobic	Alkyl
D:TRP40 - :UNK0:C25	5.25788	Hydrophobic	Pi-Alkyl
D:TRP40 - :UNK0:C25	5.11948	Hydrophobic	Pi-Alkyl

Figure 7: 2D, 3D docked images, and types of interactions between MTNB and the ligands. Seven, six, and seven interactions were identified between MTNB-Distamycin, Sunitinib, and Sorafenib. Among all the interactions, hydrogen, hydrophobic, halogen, and electrostatic interactions were found to be the most significant.

TM14A and Distamycin

8

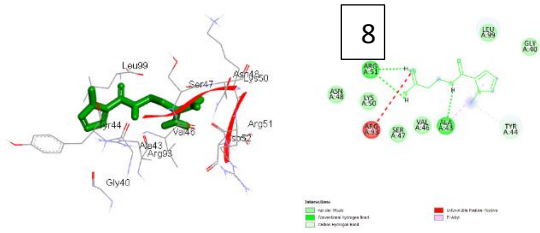

NAME	DISTANCE	CATEGORY	TYPES
:UNK0:H52 - A:ALA43:O	2.02947	Hydrogen Bond	Conventional Hydrogen Bond
:UNK0:H62 - A:ARG51:O	2.17387	Hydrogen Bond	Conventional Hydrogen Bond
:UNK0:H60 - A:ARG51:O	2.65532	Hydrogen Bond	Conventional Hydrogen Bond
:UNK0:C27 - A:TYR44:O	3.30445	Hydrogen Bond	Carbon Hydrogen Bond
:UNK0 - A:ALA43	4.35736	Hydrophobic	Pi-Alkyl

TM14A and Sunitinib

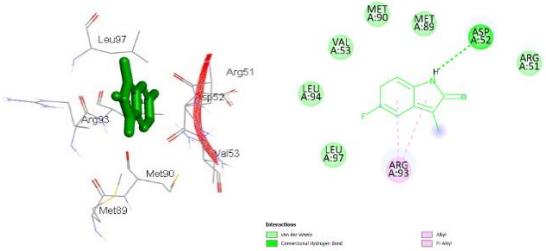

NAME	DISTANCE	CATEGORY	TYPES
:UNK0:H53 - A:ASP52:O	2.45619	Hydrogen Bond	Conventional Hydrogen Bond
A:ARG93 - :UNK0	3.96078	Hydrophobic	Alkyl
:UNK0 - A:ARG93	3.93804	Hydrophobic	Pi-Alkyl

TM14A and Sorafenib

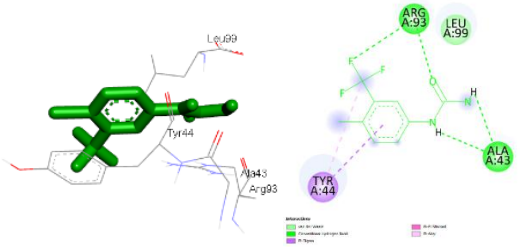

NAME	DISTANCE	CATEGORY	TYPES
:UNK0:H35 - A:ALA43:O	2.27365	Hydrogen Bond	Conventional Hydrogen Bond
:UNK0:H38 - A:ALA43:O	2.5065	Hydrogen Bond	Conventional Hydrogen Bond
A:ARG93:HH11 - :UNK0:O6	3.01724	Hydrogen Bond	Conventional Hydrogen Bond
A:ARG93:HH21 - :UNK0:O6	2.90964	Hydrogen Bond	Conventional Hydrogen Bond
A:ARG93:HH21 - :UNK0:F3	2.74642	Hydrogen Bond; Halogen	Conventional Hydrogen Bond; Halogen (Fluorine)
A:TYR44:CA - :UNK0	3.9874	Hydrophobic	Pi-Sigma
:UNK0 - A:TYR44	4.41236	Hydrophobic	Pi-Pi Stacked
A:TYR44 - :UNK0:C25	5.02093	Hydrophobic	Pi-Alkyl

Figure 8: 2D, 3D Docked Images, and Types of Interactions between TM14A and the Ligands

Five, three, and eight interactions were identified between TM14A -Distamycin, Sunitinib, and Sorafenib. Among all the interactions, hydrogen, hydrophobic, and halogen interactions were found to be the most significant.

LEG2 and Distamycin

9

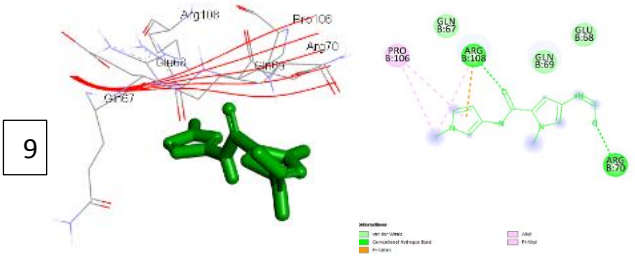

NAME	DISTANCE	CATEGORY	TYPES
B:ARG70:HN - :UNK0:O4	2.0542	Hydrogen Bond	Conventional Hydrogen Bond
B:ARG108:HH22 - :UNK0:O2	2.18242	Hydrogen Bond	Conventional Hydrogen Bond
B:ARG108:NH2 - :UNK0	3.46539	Electrostatic	Pi-Cation
:UNK0:C26 - B:PRO106	4.82708	Hydrophobic	Alkyl
:UNK0:C26 - B:ARG108	4.42139	Hydrophobic	Alkyl
:UNK0 - B:PRO106	5.38552	Hydrophobic	Pi-Alkyl

LEG2 and Sunitinib

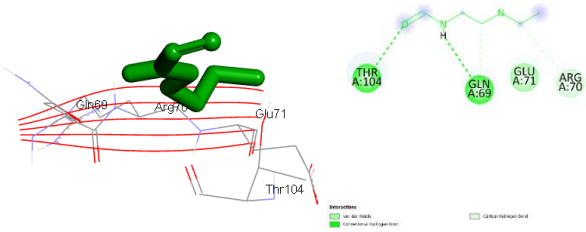

NAME	DISTANCE	CATEGORY	TYPES
:UNK0:H40 - A:GLN69:OE1	2.48412	Hydrogen Bond	Conventional Hydrogen Bond
A:THR104:HG1 - :UNK0:O2	2.76672	Hydrogen Bond	Conventional Hydrogen Bond
:UNK0:C8 - A:GLN69:OE1	3.33284	Hydrogen Bond	Carbon Hydrogen Bond
:UNK0:C14 - A:ARG70:O	3.48982	Hydrogen Bond	Carbon Hydrogen Bond

LEG2 and Sorafenib

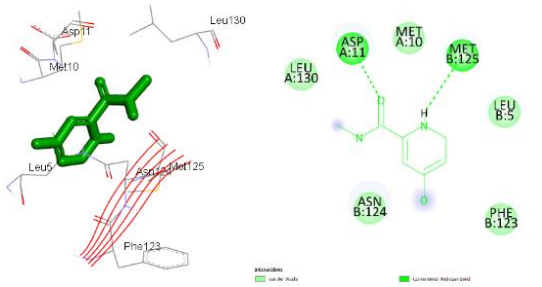

NAME	DISTANCE	CATEGORY	TYPES
:UNK0:H10 - B:MET125:O	2.32278	Hydrogen Bond	Conventional Hydrogen Bond
A:ASP11:HN - :UNK0:O7	1.85318	Hydrogen Bond	Conventional Hydrogen Bond

Figure 9: 2D, 3D Docked Images, and Types of Interactions between LEG2 and the Ligands

Six, four, and two interactions were identified between LEG2-Distamycin, Sunitinib, and Sorafenib. Among all the interactions, hydrogen, hydrophobic, and electrostatic interactions were found to be the most significant.

S10A3 and Distamycin

10

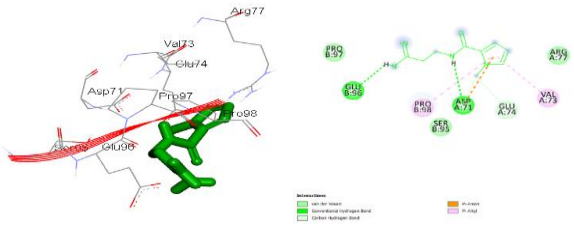

NAME	DISTANCE	CATEGORY	TYPES
:UNK0:H52 - A:ASP71:OD2	2.45135	Hydrogen Bond	Conventional Hydrogen Bond
:UNK0:H13 - B:GLU96:O	2.13201	Hydrogen Bond	Conventional Hydrogen Bond
:UNK0:C27 - A:ASP71:OD1	3.56186	Hydrogen Bond	Carbon Hydrogen Bond
:UNK0:C27 - A:GLU74:OE1	3.53891	Hydrogen Bond	Carbon Hydrogen Bond
A:ASP71:OD1 - :UNK0	4.48095	Electrostatic	Pi-Anion
:UNK0 - A:VAL73	4.86866	Hydrophobic	Pi-Alkyl
:UNK0 - B:PRO98	5.31866	Hydrophobic	Pi-Alkyl

S10A3 and Sunitinib

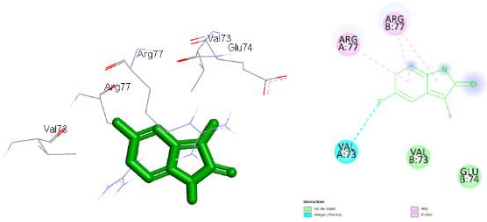

NAME	DISTANCE	CATEGORY	TYPES
A:VAL73:O - :UNK0:F1	3.18758	Halogen	Halogen (Fluorine)
A:ARG77 - :UNK0	4.33827	Hydrophobic	Alkyl
B:ARG77 - :UNK0	4.23628	Hydrophobic	Alkyl
:UNK0 - B:ARG77	5.0465	Hydrophobic	Pi-Alkyl

S10A3 and Sorafenib

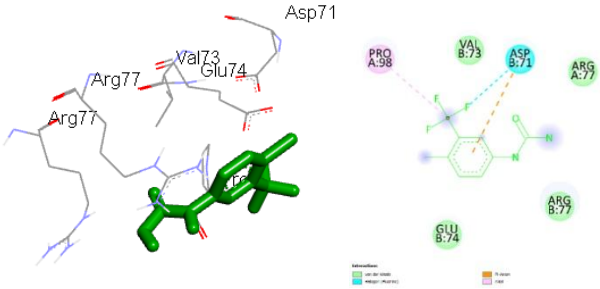

NAME	DISTANCE	CATEGORY	TYPES
B:ASP71:OD2 - :UNK0:F4	3.40158	Halogen	Halogen (Fluorine)
B:ASP71:OD1 - :UNK0	4.68492	Electrostatic	Pi-Anion
:UNK0:C25 - A:PRO98	4.37961	Hydrophobic	Alkyl

Figure 10: 2D, 3D Docked Images, and Types of Interactions between S10A3 and the Ligands

Seven, four, and three interactions were identified between S10A3-Distamycin, Sunitinib, and Sorafenib. Among all the interactions, hydrogen, halogen, hydrophobic, and electrostatic interactions were found to be the most significant.

LTC4S and Distamycin

11

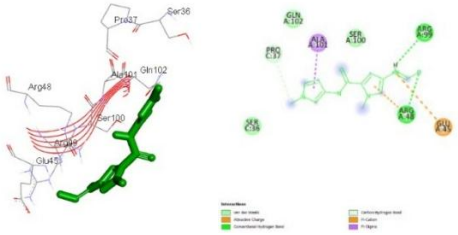

NAME	DISTANCE	CATEGORY	TYPES
:UNK0:N11 - A:GLU45:OE1	5.51337	Electrostatic	Attractive Charge
:UNK0:H58 - A:ARG99:O	2.80186	Hydrogen Bond	Conventional Hydrogen Bond
A:ARG48:HH21 - :UNK0:O4	2.52763	Hydrogen Bond	Conventional Hydrogen Bond
:UNK0:C26 - C:PRO37:O	3.68512	Hydrogen Bond	Carbon Hydrogen Bond
A:ARG48:NH1 - :UNK0	3.50209	Electrostatic	Pi-Cation
A:ALA101:CB - :UNK0	3.70364	Hydrophobic	Pi-Sigma

LTC4S and Sunitinib

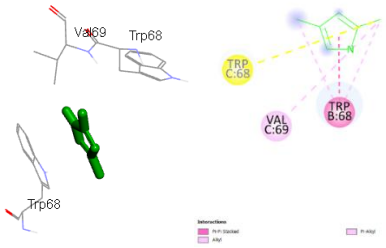

NAME	DISTANCE	CATEGORY	TYPES
:UNK0 - B:TRP68	3.63233	Hydrophobic	Pi-Pi Stacked
:UNK0 - B:TRP68	3.77142	Hydrophobic	Pi-Pi Stacked
:UNK0:C22 - C:VAL69	5.11345	Hydrophobic	Alkyl
B:TRP68 - :UNK0:C20	4.27079	Hydrophobic	Pi-Alkyl
B:TRP68 - :UNK0:C22	4.60306	Hydrophobic	Pi-Alkyl
B:TRP68 - :UNK0:C20	5.30644	Hydrophobic	Pi-Alkyl
B:TRP68 - :UNK0:C22	4.296	Hydrophobic	Pi-Alkyl
C:TRP68 - :UNK0:C22	5.48518	Hydrophobic	Pi-Alkyl

LTC4S and Sorafenib

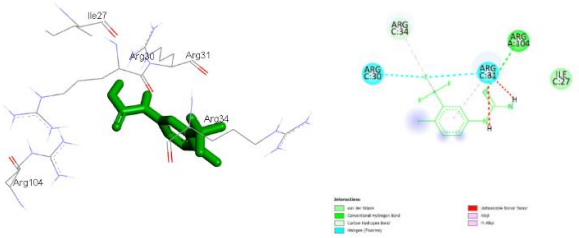

NAME	DISTANCE	CATEGORY	TYPES
A:ARG104:HH11 - :UNK0:O6	2.93938	Hydrogen Bond	Conventional Hydrogen Bond
C:ARG34:CA - :UNK0:F3	3.19546	Hydrogen Bond; Halogen	Carbon Hydrogen Bond; Halogen (Fluorine)
C:ARG30:O - :UNK0:F3	3.43226	Halogen	Halogen (Fluorine)
C:ARG31:O - :UNK0:F3	3.01161	Halogen	Halogen (Fluorine)
:UNK0:C25 - C:ARG34	3.96648	Hydrophobic	Alkyl
:UNK0 - C:ARG31	5.14952	Hydrophobic	Pi-Alkyl

Figure 11: 2D, 3D Docked Images, and Types of Interactions between LTC4S and the Ligands

Six, eight, and six interactions were identified between LTC4S -Distamycin, Sunitinib, and Sorafenib. Among all the interactions, hydrogen, halogen, hydrophobic, and electrostatic interactions were found to be the most significant.

Conclusion

One kind of malignant tumor that originates in the lung is lung carcinoma, which is another name for lung cancer. Even with treatment, just 20% of individuals survive five years following diagnosis. When it comes to treating severe instances, current medicines frequently fall short, which lowers the patient's chances of survival and lowers their quality of life. To treat the patients, new approaches must be used. One promising approach is customized medicine, which provides patients with lung cancer with specialized interventions. For in silico drug design, using bioinformatics tools offers a quicker and more effective substitute for conventional laboratory techniques.

In light of the aforementioned, the study aims to clarify the relationships between well-known anti-lung cancer medications like sorafenib, distamycin, and sunitinib and the proteins linked to lung cancer, including MTNB, TM14A, LEG2, S10A3, and LTC4S. 3D models of these proteins were created using homology modeling, and docking analyses were carried out to find important binding residues. Novel medications may successfully halt the growth of tumors by focusing on these crucial residues, providing hope for better patient outcomes.

The future of drug design using docking may focus on key topics such as quantum algorithms, cloud-based docking platforms, automated docking pipelines, Cryo-EM, customized medicine, and more, thanks to advances in technology.

References

1. Berman, H. M., Westbrook, J., Feng, Z., Gilliland, G., Bhat, T. N., Weissig, H., Shindyalov, I. N., & Bourne, P. E. (2000). The Protein Data Bank. *Nucleic acids research*, *28*(1), 235–242. https://doi.org/10.1093/nar/28.1.235
2. Boutet, E., Lieberherr, D., Tognolli, M., Schneider, M., Bansal, P., Bridge, A. J., Poux, S., Bougueleret, L., & Xenarios, I. (2016). UniProtKB/Swiss-Prot, the Manually Annotated Section of the UniProt Knowledge Base: How to Use the Entry View. *Methods in molecular biology (Clifton, N.J.)*, *1374*, 23–54. https://doi.org/10.1007/978-1-4939-3167-5_2
3. Chang, W., Tsai, M., Kuo, P., & Hung, J. (2017). Role of galectins in lung cancer (Review). Oncology Letters, 14, 5077-5084. https://doi.org/10.3892/ol.2017.6882
4. Gilad, S., Lithwick-Yanai, G., Barshack, I., Benjamin, S., Krivitsky, I., Edmonston, T. B., Bibbo, M., Thurm, C., Horowitz, L., Huang, Y., Feinmesser, M., Hou, J. S., St Cyr, B., Burnstein, I., Gibori, H., Dromi, N., Sanden, M., Kushnir, M., & Aharonov, R. (2012). Classification of the four main types of lung cancer using a microRNA-based diagnostic assay. *The Journal of molecular diagnostics: JMD*, *14*(5), 510–517. https://doi.org/10.1016/j.jmoldx.2012.03.004

5. Jang, T. H., Lin, S. C., Yang, Y. Y., Wu, S. H., Kuo, T. H., & Chuang, S. E. (2023). AXL transcriptionally up-regulates TMEM14A expression to mediate cell proliferation in non-small-cell lung cancer cells. *Biochemical and biophysical research communications*, *682*, 365–370. https://doi.org/10.1016/j.bbrc.2023.10.027
6. Kitts, P. A., Church, D. M., Thibaud-Nissen, F., Choi, J., Hem, V., Sapojnikov, V., Smith, R. G., Tatusova, T., Xiang, C., Zherikov, A., DiCuccio, M., Murphy, T. D., Pruitt, K. D., & Kimchi, A. (2016). Assembly: a resource for assembled genomes at NCBI. *Nucleic acids research*, *44*(D1), D73–D80. https://doi.org/10.1093/nar/gkv1226
7. Li, Y., Yan, B., & He, S. (2023). Advances and challenges in the treatment of lung cancer. *Biomedicine & pharmacotherapy = Biomedecine & pharmacotherapie*, *169*, 115891. https://doi.org/10.1016/j.biopha.2023.115891
8. Mary, C., Duek, P., Salleron, L., Tienz, P., Bumann, D., Bairoch, A., & Lane, L. (2012). Functional identification of APIP as human mtnB, a key enzyme in the methionine salvage pathway. *PloS one*, *7*(12), e52877. https://doi.org/10.1371/journal.pone.0052877
9. Messana, I., Manconi, B., Cabras, T., Boroumand, M., Sanna, M. T., Iavarone, F., Olianas, A., Desiderio, C., Rossetti, D. V., Vincenzoni, F., Contini, C., Guadalupi, G., Fiorita, A., Faa, G., & Castagnola, M. (2023). The Post-Translational Modifications of Human Salivary Peptides and Proteins Evidenced by Top-Down Platforms. *International Journal of Molecular Sciences*, *24*(16), 12776. https://doi.org/10.3390/ijms241612776
10. Nooreldeen, R., & Bach, H. (2021). Current and Future Development in Lung Cancer Diagnosis. *International journal of molecular sciences*, *22*(16), 8661. https://doi.org/10.3390/ijms22168661
11. Patil, R., Das, S., Stanley, A., Yadav, L., Sudhakar, A., & Varma, A. K. (2010). Optimized hydrophobic interactions and hydrogen bonding at the target-ligand interface leads the pathways of drug-designing. *PloS one*, *5*(8), e12029. https://doi.org/10.1371/journal.pone.0012029
12. Pradeepkiran, J. A., & Sainath, S. B. (Eds.). (2021). *Brucella Melitensis: Identification and Characterization of Potential Drug Targets*. Academic Press. https://www.google.co.in/books/edition/Brucella_Melitensis/GukGEAAAQBAJ?hl=en&gbpv=1&dq=11.%09Pradeepkiran%2C%20J.%20A.%20(2021).%20Brucella%20Melitensis%3A%20Identification%20and%20Characterization%20of%20Potential%20Drug%20Targets.%20Academic%20Press.&pg=PP1&printsec=frontcover
13. Sievers, F., & Higgins, D. G. (2018). Clustal Omega for making accurate alignments of many protein sequences. *Protein science: a publication of the Protein Society*, *27*(1), 135–145. https://doi.org/10.1002/pro.3290
14. Tian, W., Jiang, X., Kim, D., Guan, T., Nicolls, M. R., & Rockson, S. G. (2020). Leukotrienes in Tumor-Associated Inflammation. *Frontiers in pharmacology*, *11*, 1289. https://doi.org/10.3389/fphar.2020.01289

15. Waterhouse, A., Bertoni, M., Bienert, S., Studer, G., Tauriello, G., Gumienny, R., Heer, F. T., de Beer, T. A. P., Rempfer, C., Bordoli, L., Lepore, R., & Schwede, T. (2018). SWISS-MODEL: homology modelling of protein structures and complexes. *Nucleic acids research*, *46*(W1), W296–W303. https://doi.org/10.1093/nar/gky427
16. Wiederstein, M., & Sippl, M. J. (2007). ProSA-web: interactive web service for the recognition of errors in three-dimensional structures of proteins. *Nucleic acids research*, *35*(Web Server issue), W407–W410. https://doi.org/10.1093/nar/gkm290
17. Ye, B., Tian, W., Wang, B., & Liang, J. (2024). CASTpFold: Computed Atlas of Surface Topography of the universe of protein Folds. *Nucleic acids research*, *52*(W1), W194–W199. https://doi.org/10.1093/nar/gkae415
18. Yoder, L. H. (2006). An overview of lung cancer symptoms, pathophysiology, and treatment. *Medsurg Nursing*, *15*(4), 231. https://citeseerx.ist.psu.edu/document?repid=rep1&type=pdf&doi=e3b787dc121c9e0c7ed5fc8b421e2262793530e1